


Two-step Structural Design of Mesh Antennas for High Beam Pointing Accuracy

Shuxin ZHANG^{1,2} · Jingli DU¹ · Wei WANG¹  · Xinghua ZHANG² · Yali ZONG¹

Received: 9 May 2016 / Revised: 18 February 2017 / Accepted: 2 April 2017 / Published online: 21 April 2017
© The Author(s) 2017. This article is an open access publication

Abstract A well-designed reflector surface with high beam pointing accuracy in electromagnetic performance is of practical significance to the space application of cable mesh reflector antennas. As for space requirements, circular polarizations are widely used in spaceborne antennas, which usually lead to a beam shift for offset reflectors and influence the beam pointing accuracy. A two-step structural design procedure is proposed to overcome the beam squint phenomenon for high beam pointing accuracy design of circularly polarized offset cable mesh reflectors. A simple structural optimal design and an integrated structural electromagnetic optimization are combined to alleviate the beam squint effect of circular polarizations. It is implemented by cable pretension design and adjustment to shape the offset cable mesh surface. Besides, in order to increase the efficiency of integrated optimization, an update Broyden-Fletcher-Goldfarb-Shanno (BFGS) Hessian matrix is employed in the optimization iteration with sequential quadratic programming. A circularly polarized offset cable mesh reflector is utilized to show the feasibility and effectiveness of the proposed procedure. A high beam pointing accuracy in order of 0.0001° of electromagnetic performance is achieved.

Keywords Cable mesh reflector antennas · Structural design · Beam squint · Beam pointing accuracy

1 Introduction

In recent years, the stringent requirements on large space reflectors become demanding for high electromagnetic performance [1]. As for space applications, circular polarizations are usually used in spaceborne antennas. With circularly polarized feeds, there exists a beam squint phenomenon in offset reflector antennas [2]. The squint angle, which is manifested by a small beam shift of the radiation pattern in the plane perpendicular to the principal offset plane, can significantly affect the beam pointing accuracy. As one of the most widely used space antennas, cable mesh reflector antenna has attracted much attention due to its advantages of large diameter, light weight, and reasonable cost [3]. Similarly with the smooth solid reflectors, the beam squint phenomenon can also be observed in offset cable mesh reflector antennas with reflecting mesh leakage [4, 5]. The beam squint angle should be taken into account for space applications such as satellite communications, deep-space telemetry, and radio astronomy [2], which concentrate more on beam pointing accuracy. With the stringent requirements on space reflector antennas, the compensation technology to overcome the antenna pattern degradation including beam squint to achieve high pointing accuracy becomes more demanding [6].

Since the simple formula which accurately predicts the squint angle in circularly polarized offset reflectors was proposed by ADATIA and RUDGE [7], the beam squint phenomenon and its compensation method have attracted many authors' interests. A squint compensation method by properly tilting the feed to make the interpreted angle between the incident beam and the radiated beam zero is a natural choice for symmetrical reflectors with off-focus feeds [8]. A squint free approach for symmetrical dual reflector antennas is also proposed by properly choosing

✉ Wei WANG
wwang@xidian.edu.cn

¹ Key Laboratory of Electronic Equipment Structure Design of Ministry of Education, Xidian University, Xi'an 710071, China

² Qian Xuesen Laboratory of Space Technology, China Academy of Space Technology, Beijing 100094, China

geometrical parameters [9]. Furthermore, XU and RAHMAT-SAMII [2] summarized the beam squint compensation methods, and proposed a compensation technology by optimally displacing circularly polarized feeds in the perpendicular plane to obtain high beam pointing accuracy. However, these methods in Refs. [2, 7–9] are presented from the simple electromagnetic disciplinary, and they are just practical for undistorted reflectors in the nominal state for preliminary design. In actual engineering, space reflectors including cable mesh antennas are easily susceptible to surface distortion under thermal load and other impacts, which enlarge the beam squint angle and seriously affect the beam pointing accuracy. Simply displacing and tilting the antenna feed cannot thoroughly compensate the distorted electromagnetic performance in actual engineering. Another consideration should be taken into account is that feed remains on focus with a satisfactory reflector surface is preferred due to the limited size in satellites. How to produce a cable mesh reflector with high beam pointing accuracy in electromagnetic performance is an urgent problem for space applications.

As for structural design of cable mesh reflectors, pretension design of cable nets is an important process to obtain the required reflector surface. Recently, there are several methods which investigate the form-finding analysis for cable mesh reflectors, such as the method presented by TANAKA, et al [10], optimal design method of initial surface in Ref. [11], simple technique in Ref. [12], numerical form-finding method proposed by MORTEROLLE, et al [13] to ensure uniform tension, form-finding analysis with PZT actuators [14] and pretension design under multi-uncertainty [15]. These methods aim to design a surface profile with minimum or zero root-mean-square (rms) error to ensure its surface accuracy. Although the reflector shape can be obtained with high surface accuracy by these methods, its beam pointing accuracy cannot be easily guaranteed, even for circularly polarized feeds. Thus, there rises a problem that is it possible to provide a pretension structural design considering electromagnetic performance to obtain high beam pointing accuracy for circularly polarized feeds? The integrated structural electromagnetic design concept [16, 17] inspires us with a combined procedure, which makes a pretension design from multidisciplinary viewpoint of structure and electromagnetism.

The main purpose of this paper is to present a two-step structural design technology for circularly polarized offset cable mesh reflectors with high beam pointing accuracy. The two-step pretension design combines a simple structural design and an integrated structural electromagnetic optimization. With this technology, high electromagnetic performance especially high beam pointing accuracy can

be achieved in the antenna structural design. This technology not only can compensate the beam squint angle of circular polarizations, but also can produce a well-designed cable mesh reflector with on-focus feeds. Comparing with the compensation methods proposed by electromagnetism designers, the limited weakness of aforementioned methods can be overcome.

This paper is organized as follows. Section 2 of this study outlines the procedure of the two-step structural design technology. In this technology, an update Broyden-Fletcher-Goldfarb-Shanno (BFGS) Hessian matrix is employed to increase the efficiency of optimization iteration. In section 3, a circularly polarized offset cable mesh reflector is utilized to show the feasibility and effectiveness of this procedure with an on-focus feed to achieve high beam pointing accuracy in electromagnetic performance. The major achievements are summarized in section 4.

2 Two-step Structural Design Procedure

The cable mesh reflector usually consists of front cables, rear cables, tie cables, reflective mesh, and ring truss. Its pretension design aims to find a reasonable cable tension distribution, which offers rigidity to form the required parabolic surface. The present two-step structural design technology incorporates a simple structural form-finding design and an integrated structural electromagnetic optimization to achieve high beam pointing accuracy. The simple structural form-finding design starts from the preliminary stage considering surface error requirement. As for the cable mesh reflector, the surface rms error can be expressed as [18]

$$\delta_{\text{rms},z} = \frac{1}{16\sqrt{15}f} \frac{l^2}{T} \left(1 + 0.33 \frac{N_m l}{T} \right), \quad (1)$$

where $\delta_{\text{rms},z}$ is the surface rms error in z direction, f is the focal length, l is the cable dimension, N_m is the mesh tension, and T is the surface cable tension.

Usually, for a preliminary estimation, the surface cable tension T will be set equal to 10 times [19] the mesh tension N_m multiplied by the side length l to suppress pillow deformation [20]. Such that, given the working wavelength (or frequency) and required surface rms error (usually smaller than $1/50$ wavelength), the surface cable length can be determined as

$$l \leq \sqrt{16\sqrt{15}f\delta_{\text{rms},z}} / 1.033. \quad (2)$$

After determining the surface cable length l , the number division in radius can be obtained in preliminary design. Thus, with the required parabolic surface equation, the

predesigned surface nodal positions in front and rear cable nets can be calculated.

In the following structural design, in order to obtain a circularly polarized cable mesh reflector with high beam pointing accuracy, the predesigned nodes are firstly assumed in the nominal undistorted state. As mentioned before, there exists a beam squint phenomenon for this offset antenna. Then, with the integrated structural electromagnetic optimization, the beam squint phenomenon will be compensated.

Supposing that free node i is connected to node t by a cable, the equilibrium equation in z direction for node i can be derived as [21]

$$\sum_t \frac{T_{it}}{l_{it}}(z_i - z_t) = 0, \quad (3)$$

where T_{it} is the tension in element it and l_{it} is the cable length of element it , z_i and z_t are the coordinates in z direction for node i and t , respectively.

Collecting the equilibrium equations for all free nodes in x , y , and z directions, a matrix form equation can be obtained as follows:

$$\mathbf{A}_{3n \times m} \mathbf{T}_{m \times 1} = 0, \quad (4)$$

where \mathbf{A} is the equilibrium matrix, \mathbf{T} is the column vector of cable tensions, n is the number of free nodes and m is the number of cables. Usually, for cable net reflectors, the matrix form equilibrium Eq. (4) is statically indeterminate, which has many different cable tension distributions to satisfy this equation.

To determine the cable tension, the Singular Value Decomposition (SVD) is performed on the equilibrium matrix \mathbf{A} , and the cable tensions can be expressed as the linear combination of the independent states of self-stress [22]. With optimizing the combination coefficients of multiple states of self-stress, the cable tensions can be obtained in this nominal state.

The optimization model of this structural design can be written as

$$\begin{aligned} \text{find } & \boldsymbol{\alpha} = (\alpha_1, \alpha_2, \dots, \alpha_p)^T, \\ \text{min } & \|\mathbf{T} - \mathbf{T}_0\|, \\ \text{s.t. } & \mathbf{A}_{3n \times m} \mathbf{T}_{m \times 1} = 0, \\ & \mathbf{T} = \mathbf{V}_{m \times p} \cdot \boldsymbol{\alpha}_{p \times 1}, \\ & \underline{\mathbf{T}} \leq \mathbf{T} \leq \bar{\mathbf{T}}, \end{aligned} \quad (5)$$

where $\boldsymbol{\alpha}$ is the column vector of combination coefficients, p is the number of independent states of self-stress, \mathbf{T}_0 is the column vector of mean values of cable tensions, \mathbf{V} is the matrix of independent states of self-stress, $\underline{\mathbf{T}}$, $\bar{\mathbf{T}}$ are the lower and upper limits of cable tensions, respectively. The object in this model is to find a uniform tension distribution for cable mesh reflectors. With this optimization, the pre-tension design of cable nets can be achieved. Other form-finding methods can also be employed in the first step.

The next step is to improve the electromagnetic performance with high beam pointing accuracy. In the beginning, all of the surface nodes are in nominal state, and poor beam pointing accuracy can be observed under circular polarizations. The high beam pointing accuracy is optimized by an integrated structural electromagnetic design, which directly chooses the electromagnetic performance as design object. The integrated implementation is accomplished by altering some cable lengths, usually tie cables, which shapes the front cable surface to obtain high beam pointing accuracy. This implementation is similar with the shape control concept [23], and beam pointing accuracy makes it different. The integrated structural electromagnetic optimization minimizing beam squint angle can be expressed as

$$\begin{aligned} \text{find } & \mathbf{l} = (l_1, l_2, \dots, l_N)^T, \\ \text{min } & \theta_0, \\ \text{s.t. } & D(\mathbf{l}) \geq \underline{D}, \\ & \underline{\mathbf{T}} \leq \mathbf{T} \leq \bar{\mathbf{T}}, \\ & \underline{\mathbf{l}} \leq \mathbf{l} \leq \bar{\mathbf{l}}, \end{aligned} \quad (6)$$

where \mathbf{l} is the column vector of dimensions of altered tie cables, N is the number of tie cables, θ_0 is the beam squint angle represents beam pointing accuracy, D is the maximum directivity with its lower limit \underline{D} , $\underline{\mathbf{l}}$, $\bar{\mathbf{l}}$ are the lower and upper limits of design variables, respectively. The directivity constraint is added in the optimization model to ensure better electromagnetic performance during iterations. Strictly speaking, other electromagnetic performance can also be added into the constraints in the optimization model.

In this solution procedure, in order to avoid the computation of directivity values at different radiation angles during iterations to determine the beam pointing direction, the optimization model in Eq. (6) can be converted to a new procedure which maximizes the boresight directivity at boresight direction (0, 0). It is rewritten as

$$\begin{aligned} \text{find } & \mathbf{l} = (l_1, l_2, \dots, l_N)^T, \\ \text{min } & -D(0, 0), \\ \text{s.t. } & D(0, 0) \geq \underline{D}, \\ & \underline{\mathbf{T}} \leq \mathbf{T} \leq \bar{\mathbf{T}}, \\ & \underline{\mathbf{l}} \leq \mathbf{l} \leq \bar{\mathbf{l}}, \end{aligned} \quad (7)$$

where $D(0, 0)$ is the boresight directivity and the boresight direction is defined at (0, 0). The equivalence of the optimization model in Eqs. (6) and (7) is easily understood from the viewpoint of electromagnetism and it will be shown in section 3.

In order to solve this optimization model in Eq. (7), sensitivity analysis is employed in this implementation. The optimization model can be converted into a new one by expanding the object into a second-order Taylor series

and the constraint into a first-order Taylor series. The new optimization model in the i th iteration can be illustrated as

$$\begin{aligned} \text{find } \Delta \mathbf{l} &= (\Delta l_1, \Delta l_2, \dots, \Delta l_N)^T, \\ \text{min } -D(0,0) &= -D^{(i)} - \mathbf{G}^T \Delta \mathbf{l} - \frac{1}{2} \Delta \mathbf{l}^T \mathbf{B} \Delta \mathbf{l}, \\ \text{s.t. } D^{(i)} + \mathbf{G}^T \Delta \mathbf{l} - \underline{D} &\geq 0, \\ \underline{\mathbf{T}} &\leq \mathbf{G}_t^T \Delta \mathbf{l} + \mathbf{T}^{(i)} \leq \bar{\mathbf{T}}, \\ \underline{\mathbf{l}} - \mathbf{l}^{(i)} &\leq \Delta \mathbf{l} \leq \bar{\mathbf{l}} - \mathbf{l}^{(i)}, \end{aligned} \quad (8)$$

where $\Delta \mathbf{l}$ is the increment column vector of cable dimensions, $\mathbf{l}^{(i)}$ is the vector of cable dimensions in the i th iteration, $D^{(i)}$ is the boresight directivity in the present state, $\mathbf{T}^{(i)}$ is the vector of cable tensions in the present state, \mathbf{G} is the gradient vector of boresight directivity with respect to cable dimensions, \mathbf{B} is the BFGS update Hessian matrix, \mathbf{G}_t is the gradient matrix of cable tensions with respect to cable dimensions.

The derivation of \mathbf{G} is based on two sensitivities - one is the electromagnetic sensitivity of boresight directivity with respect to surface nodal displacements, and the other is the structural sensitivity of surface nodal displacements with respect to cable dimensions. Its expression is illustrated in Refs. [17, 23]. The constraint gradient matrix \mathbf{G}_t is based on structural sensitivity analysis of cable tensions with respect to cable dimensions [23]. By using the nonlinear optimization function—*quadprog* in MATLAB, this optimization model can be solved.

Besides, in order to increase the efficiency of this optimization and avoid the direct computation of Hessian matrix, an update BFGS formula [24] is employed in the iteration. The approximation to Hessian matrix in the i th iteration is denoted by \mathbf{B}_i , and the well-known BFGS formula is defined as [24]

$$\mathbf{B}_{i+1} = \mathbf{B}_i - \frac{\mathbf{B}_i \mathbf{P}_i \mathbf{P}_i^T \mathbf{B}_i}{\mathbf{P}_i^T \mathbf{B}_i \mathbf{P}_i} + \frac{\mathbf{Y}_i \mathbf{Y}_i^T}{\mathbf{Y}_i^T \mathbf{P}_i}, \quad (9)$$

where \mathbf{P}_i is the difference of design variables between last two iterations, and \mathbf{Y}_i is the difference of the gradient vectors of object function between last two iterations.

$$\mathbf{P}_i = \Delta \mathbf{l}^{(i)}, \quad (10)$$

$$\mathbf{Y}_i = \mathbf{G}^{(i+1)} - \mathbf{G}^{(i)}, \quad (11)$$

where $\Delta \mathbf{l}^{(i)}$ is the difference of cable dimensions between last two iterations, $\mathbf{G}^{(i)}$ is the gradient vector of boresight directivity with respect to cable dimensions in the i th iteration. The gradient vector is updated by sensitivity analysis during the iterations [25].

By adding the solution of the optimization model in Eq. (8) to the cable dimensions in the present state, the updated column vector of cable dimensions in the next iteration can be obtained as

$$\mathbf{l}^{(i+1)} = \mathbf{l}^{(i)} + \Delta \mathbf{l}^{(i)}. \quad (12)$$

The procedure of this two-step structural design technology is shown in Fig. 1. It is described as follows.

- Step 1 Provide the initial parameters of cable mesh reflector, including the diameter, focal length, offset height, mesh tension, working frequency, and feed polarization;
- Step 2 Perform the preliminary design by the relationship between surface rms error and cable length;
- Step 3 Obtain the equilibrium equation in the nominal state;
- Step 4 Perform SVD operation to obtain the independent states of self-stress;
- Step 5 Solve the pretension optimization model in (5);
- Step 6 Perform structural and electromagnetic (EM) sensitivity analysis;
- Step 7 Approximate Hessian matrix using BFGS update formula;
- Step 8 Update cable dimensions;
- Step 9 Obtain the structural and EM performance in the present state;

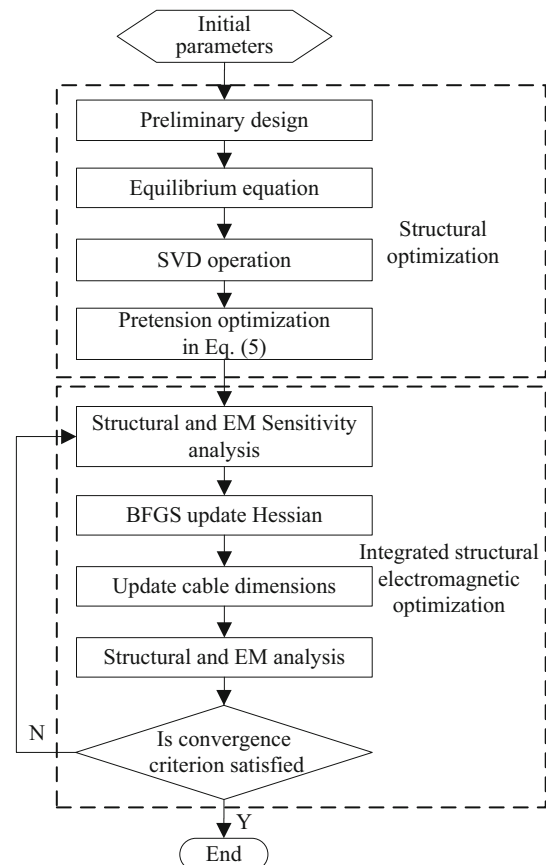


Fig. 1 Flow-chart of the two-step structural design

Step 10 Does the EM performance satisfy the convergence criterion? If no, go to Step 6, otherwise, export the optimum design.

It should be mentioned that the implementation from Step 3 to Step 5 belongs to the structural pretension design, and the procedure from Step 6 to Step 10 is a typical integrated structural electromagnetic optimization design. With this two-step structural design, an offset cable mesh reflector with high beam pointing accuracy under circular polarization will be obtained.

3 Simulation and Application

A circularly polarized offset cable mesh reflector antenna is employed in this section. Parameters are listed below in Table 1 including the cable mesh reflector geometry parameters, and feed parameters. The antenna is working under right-hand circularly polarized (RCP) illumination. Its configuration is shown in Fig. 2(a). The object is to perform a pretension design of this cable reflector with high beam pointing accuracy under the circular polarization.

The cable mesh reflector specifications are given in Table 1.

According to the surface rms error requirement, the aperture is divided into 5 segments in radius. There are 85 free nodes, 36 fixed nodes, 288 cables in each net and 85 tie cables in the whole cable net structure, which form triangular facets to approximate the surface. This configuration is illustrated in Fig. 2(b), where solid line represents the cables and dashed line for ring truss. Meanwhile, the surface cable tension T should be about 10 times the mesh tension N_m multiplied by the side length l , and such that the tie cable tension T_{tie} is about $T_{tie} = 1.57l/f = 5$ N by the equilibrium relation addressed in [19]. In the following structural pretension design optimization, the mean value of tie cable tensions is set as 5 N and among the constraints, the cable tensions should be positive ($T > 0$) and not exceed the upper limit of 50 N ($T < 50$ N). The cable tension distribution of initial nominal state (dashed line) after structural pretension design is shown in Fig. 3, where the cable numberings from 1 to 288 denote front cables, 289 to 576 for rear cables and the rest are for tie cables. From this figure, it shows that each tie cable tension is arranged as 5 N.

With the structural pretension design, a surface with uniform tie cable tension distribution can be obtained and all of the surface nodes are located at their nominal states. In the next, the electromagnetic performance is examined for this circular polarization. Beam squint occurs in this circularly polarized offset cable mesh reflector antenna. In the nominal state for RCP feed illumination, there exists a

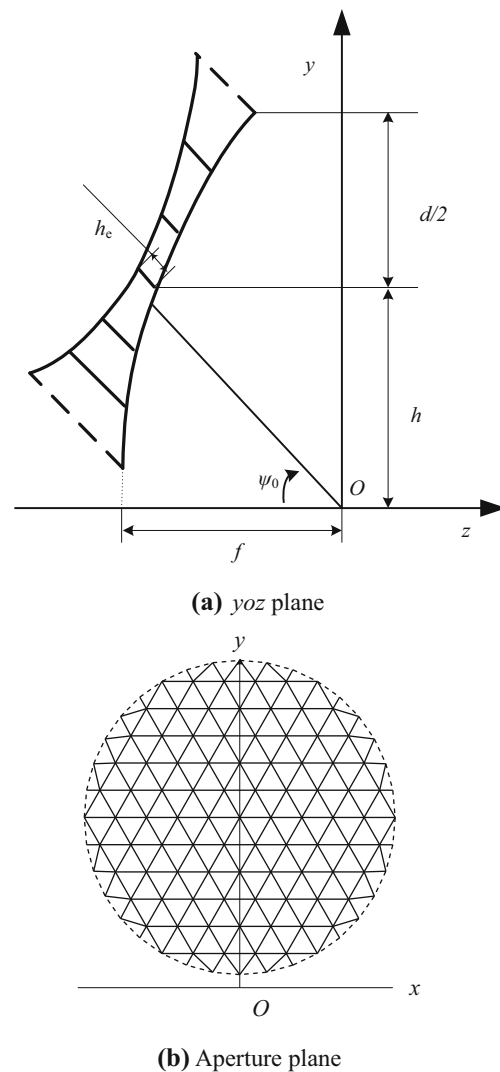


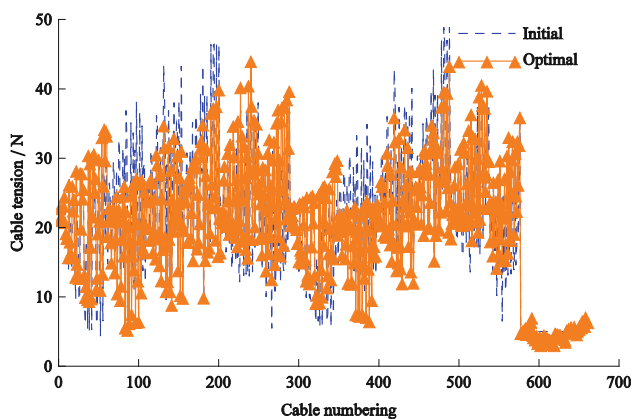
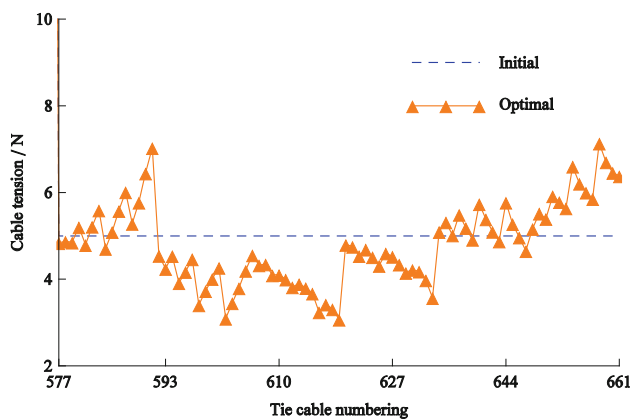
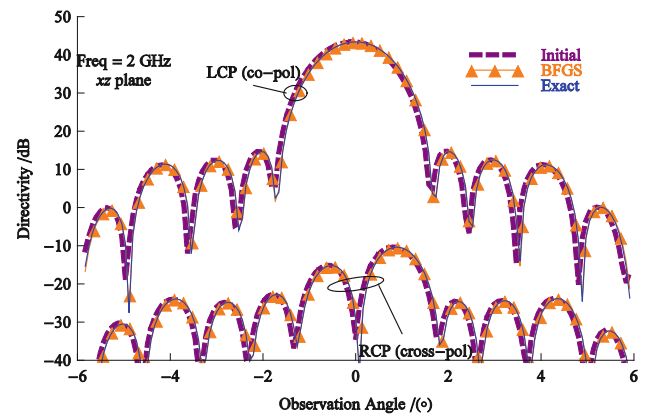
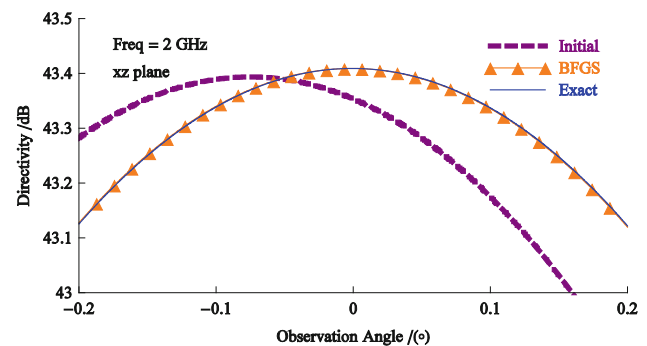
Fig. 2 Geometry of an offset cable mesh reflector antenna in the nominal state

linear phase shift across the reflector aperture and the phase in the left side aperture region is lagging compared with the phase in the right side aperture region. The radiated left-hand circularly polarized (LCP) beam, which is launched from the RCP feed and reflected by this reflector, squints toward the right in xz plane and produces a negative squint angle.

The far field pattern in xz plane for the initial nominal state is shown in Fig. 4 with a close-up view by dashed line. The beam squint angle influences antenna beam pointing accuracy, and should be suppressed. Using the integrated structural electromagnetic optimization described in section 2, its beam pointing accuracy will be improved. The convergence criterion of the integrated optimization is set as $10\lg D^{(i)} - 10\lg D^{(i-1)} \leq \varepsilon$, where ε is a small number. In the optimization, the lower limit \underline{D} of maximum directivity is set as the nominal directivity

Table 1 Cable mesh reflector specifications

Items	Value or character
Reflector type	Single offset parabola
Aperture diameter d/m	9.23
Focal length f/m	6
Offset height h/m	5
Minimum distance between the front and rear cable nets h_c/m	0.2
Young's modulus of cables E/GPa	20
Cable cross-sectional area A/mm^2	3.14
Mesh tension $N_m/(N\ m^{-1})$	2.0
Frequency/GHz	2
Cosine-Q feed $Q_x\ Q_y$	8.338
Polarization	RCP
Feed tilt angle $\psi_0/(^{\circ})$	41.64
Feed position	On focus

**(a)** Cable tensions**(b)** Tie cable tensions**Fig. 3** Cable tension distribution of the initial nominal state and optimal state (RCP feed)**(a)** Far field pattern (RCP)**(b)** Close-up view pattern (RCP)**Fig. 4** Comparative results of far field patterns with RCP illumination

($\bar{D} = 43.353\ 3$), the cable tension constraints are same as the first step, and the tie cable length limits are set as $l^{(i)} - 2\text{mm}$ and $l^{(i)} + 2\text{mm}$, respectively.

In the beginning, the equivalence of optimization model in Eq. (6) and Eq. (7) is illustrated through simulations with different convergence criteria. Table 2 shows the optimal results of boresight directivity, squint angle and iteration number with different convergence criteria. As the value of ε decreases, the optimal results will provide a higher boresight directivity, a smaller squint angle and cost a larger iteration number. Although the beam squint angle constraint is not added in the optimization model Eq. (7), the squint angle constraint can be checked after iterations;

Table 2 Optimal results with different convergence criteria

Convergence criterion/ ε	10^{-4}	10^{-5}	10^{-6}	Nominal state
Boresight directivity/dB	43.408 1	43.408 7	43.408 9	43.353 3
Squint angle/($^{\circ}$)	-0.007 4	-0.002 9	-0.000 6	-0.075 1
Iteration number	72	82	96	—

if the squint angle constraint is not satisfied, decrease the value of ε and perform another optimization design. As for some satellite applications, the beam squint angle below 0.001° is allowable, so the convergence criterion is chosen as 10^{-6} in the following simulation. Once the boresight directivity reaches the extremely maximum value with sufficient accuracy, the beam squint angle will decrease down to an allowable value. This can be explained in electromagnetism that as the optimization performs, a better uniform aperture phase distribution will be obtained, and the uniform aperture phase distribution will produce a maximum directivity in boresight direction and the radiated beam will thus direct to the boresight, which makes the beam squint angle zero.

Figure 4(a) shows the copolarization(co-pol) and cross-polarization(cross-pol) far field patterns of the initial nominal state (dashed line), the optimal state by BFGS Hessian (marked line), and the optimal state by exact Hessian (solid line) in xz plane for RCP feed illumination. The close-up view is shown in Fig. 4(b). The major parameters are shown in Table 3. The procedure of BFGS update Hessian provides a little lower maximum directivity (43.408 8 dB) and a larger beam squint angle (-0.0014°) than that of the exact one. The contour beam pattern of the optimal state by BFGS Hessian is illustrated in Fig. 5. The iteration history of boresight directivity with RCP illumination is shown in Fig. 6, and it also took a less iteration number (87) using the BFGS update formula than that of the exact Hessian procedure (96). In the meantime, the optimization procedure by BFGS update formula also cost less time (421.428 s) than that of the exact one (501.024 s) with RCP illumination.

The contour plot of surface nodal z -displacements (Unit: m) in the optimal state is shown in Fig. 7. From Fig. 7, it can be seen that the optimal structural design provides a tilt-like surface deformation- the surface nodal displacements are increased from negative values in right and lower region to positive values in left and upper region. This is due to the fact that in the initial nominal state, the phase in the left side aperture region is lagging compared with the phase in the right side aperture region, and the procedure provides an optimal tilt-like surface to achieve a uniform

Table 3 Major parameters of far field patterns with RCP illumination

Items	Max Directivity/ dB	HPBW ^a / (°)	Left sidelobe Level/dB	Right Sidelobe level/dB	Beam Squint/ (°)
Exact Hessian	43.408 9	1.261	-28.754	-28.787	-0.0006
BFGS Hessian	43.408 8	1.261	-28.899	-28.652	-0.0014

^a Half power beam width (HPBW)

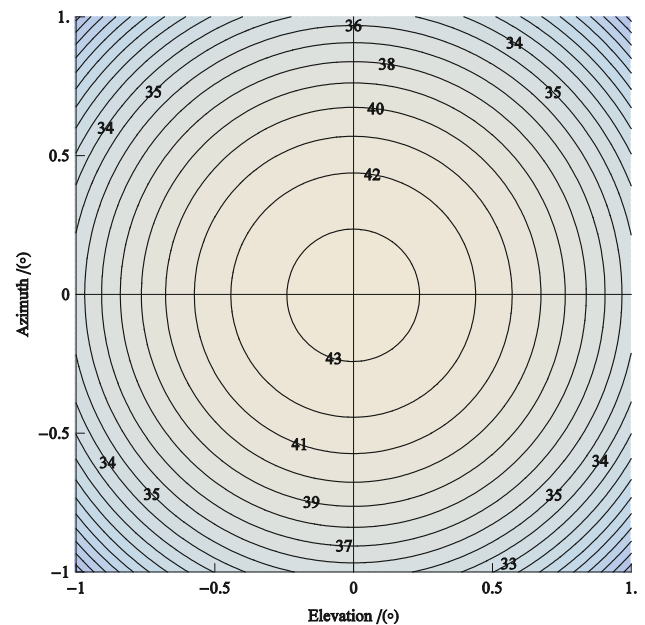


Fig. 5 Contour beam pattern of the optimal state (RCP feed)

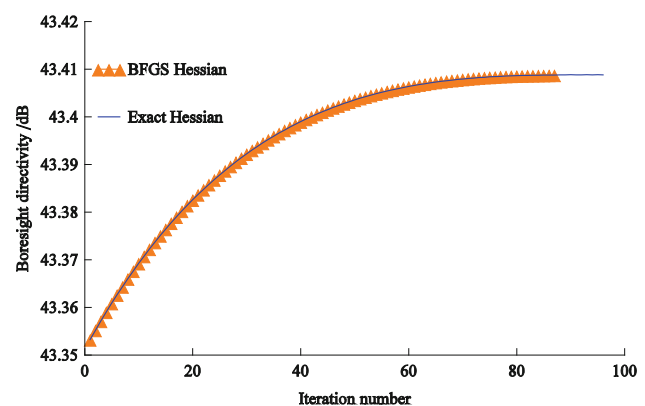


Fig. 6 Boresight directivity during iterations (RCP feed)

phase distribution which makes the nodes in left and upper region positive z -displacements and the nodes in right and lower region negative z -displacements. The compressed contour lines near the aperture rim in Fig. 7 are due to the fact that the ring truss represented by dashed line in Fig. 2 is fixed and unchanged during iterations. The cable tensions of the optimal state are shown in Fig. 3 with triangular marked line. The tensions in tie cables are rearranged with a maximum value of 7.14 N, a minimum value of 3.07 N, and an average value of 4.82 N.

Considering the far field patterns in Fig. 4 and the optimization model in Eq. (7), it can be seen that although the constraints of the other electromagnetic performance such as sidelobe levels and cross-polarization are not added in the optimization model, the simulation result in Fig. 4 shows very satisfactory far field patterns in sidelobes and cross-polarization pattern. This can be explained that the

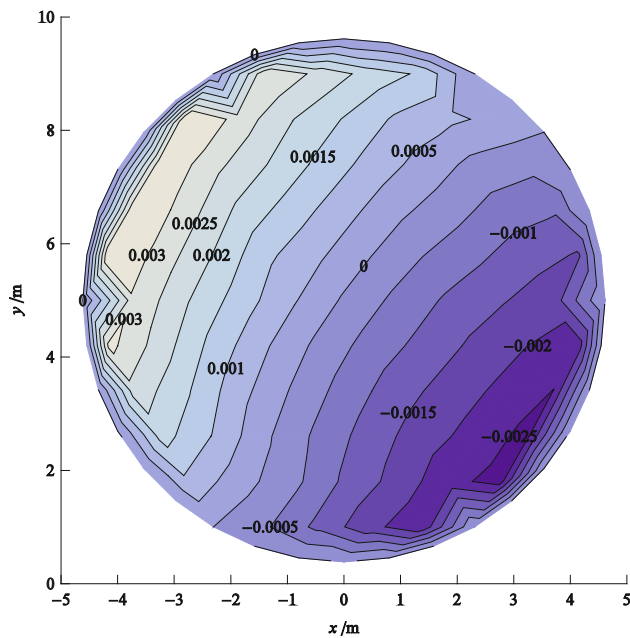
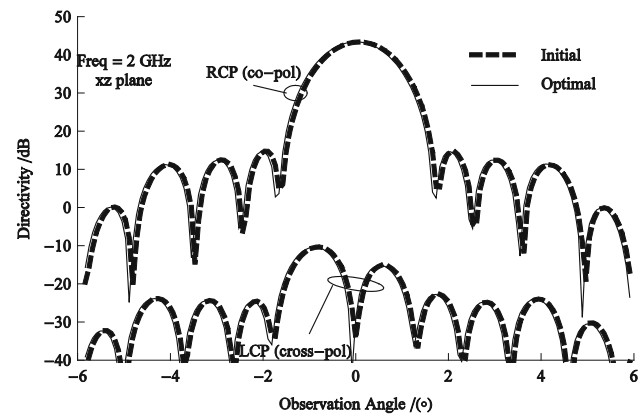


Fig. 7 Contour plot of surface nodal z-displacements in the optimal state (RCP feed)

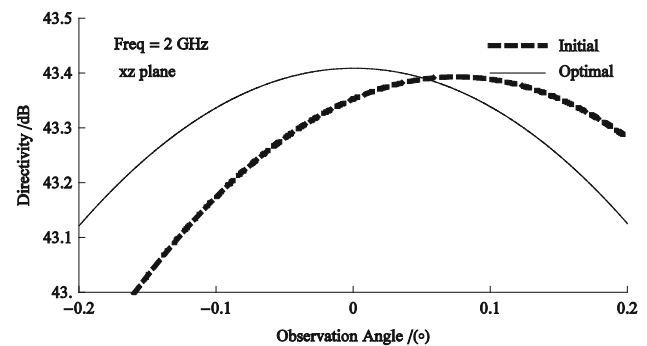
effects of surface error on boresight directivity and the other performance are harmonious; the nonuniform phase distribution will produce a lower directivity and higher sidelobe levels; as the phase distribution across the reflector aperture becomes more uniform, the antenna electromagnetic performance including boresight directivity, sidelobe levels and cross-polarization will become better.

Similarly, the optimal results for LCP feed illumination can also be predicted by symmetry. Another simulation with a LCP feed verifies the prediction. Fig. 8(a) shows the far field patterns of the initial nominal state (dashed line) and optimal state (solid line) in xz plane for LCP feed illumination and its close-up view is shown in Fig. 8(b). In the initial nominal state for LCP feed illumination, the phase in the left side aperture region is leading compared with the phase in the right side aperture region, which causes the radiated RCP beam to squint toward the left in xz plane and produces a positive squint angle. The contour plot of surface nodal z-displacements in the optimal state for LCP feed illumination is shown in Fig. 9. The optimal structural design also provides a tilt-like surface deformation- the surface nodal displacements are increased from negative values in left and lower region to positive values in right and upper region. The deformation in the optimal state for LCP feed illumination is symmetrical with the optimal surface for RCP feed illumination about the offset axis (y).

From the application, it can be concluded that a well-designed cable mesh reflector with high beam pointing accuracy in electromagnetic performance is obtained by a



(a) Far field pattern (LCP)



(b) Close-up view pattern (LCP)

Fig. 8 Far field patterns of the initial nominal state and optimal state (LCP feed)

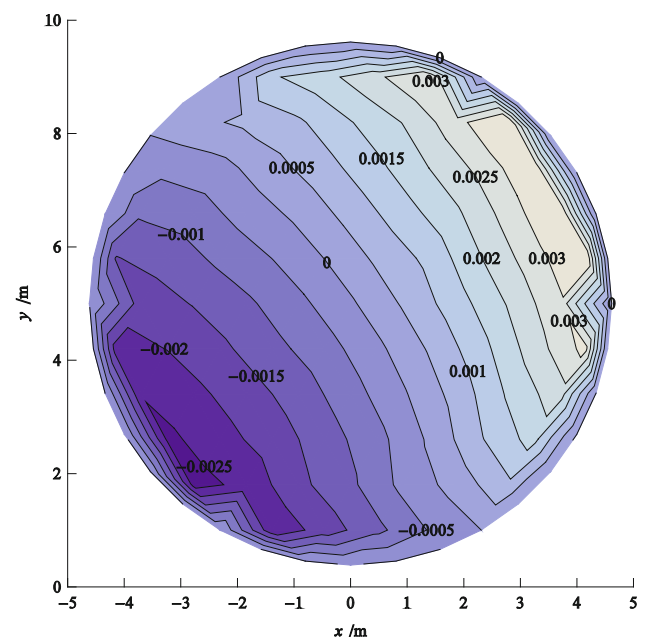


Fig. 9 Contour plot of surface nodal z-displacements in optimal state (LCP feed)

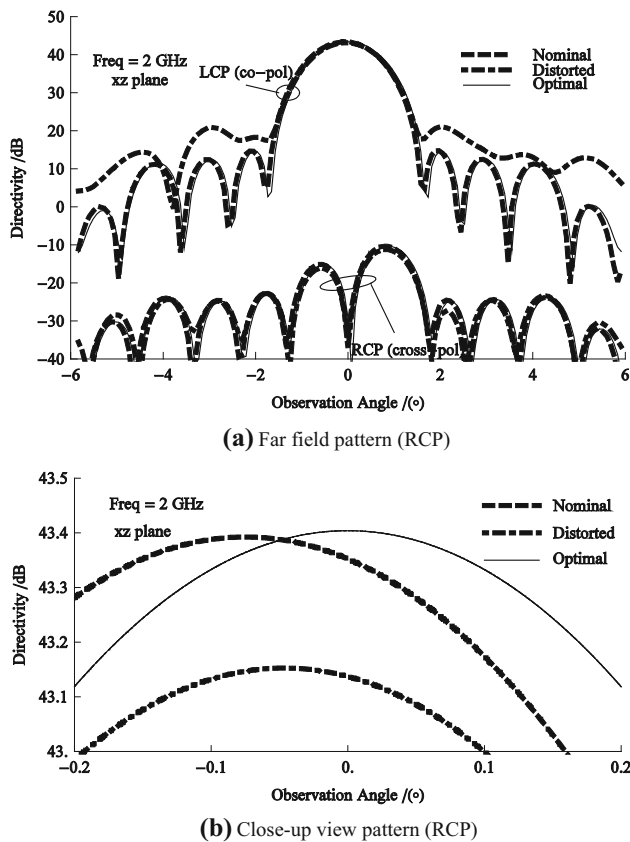


Fig. 10 Far field patterns of the nominal state, the distorted state and the optimal state (RCP feed)

two-step structural design. This beam squint free technology is accomplished by structural design to shape surface with a uniform phase distribution in the aperture plane, and the linear phase shift caused on the polarized components of the incident field is thus reduced. This procedure benefits the radiation pattern with no need to displace feed position and orientation.

Furthermore, in order to show the versatility of the proposed method for distorted cable mesh reflectors in actual engineering, the technology is added into the shape control of a distorted cable mesh reflector with RCP feed illumination. Fig. 10(a) shows the far field patterns of the nominal state (dashed line), the distorted state (dot dashed) and the optimal state (solid line) in xz plane for RCP feed illumination, and the close-up view is illustrated in Fig. 10(b). The boresight directivity increases from 43.13 dB in the distorted state to 43.40 dB in the optimal state, and the squint angle decreases from 0.046° in the distorted state to 0.0003° in the optimal state. It is shown that the technology can not only compensate the beam squint in the nominal state for circularly polarized cable mesh reflectors, but also improve the deterioration performance of distorted reflectors.

From the above comparative simulation between BFGS update Hessian matrix and exact Hessian matrix by second-order derivative, it can be seen that the BFGS approximation matrix can provide less iteration time and a little worse electromagnetic performance with maximum directivity in accuracy of 0.0001 dB than the exact one in the cable mesh reflector antenna design.

Compared with the previous compensation methods, this technology can not only compensate the beam squint angle with an on-focus circular polarized feed, but also provide a well-designed surface with high beam pointing accuracy considering actual engineering. The mentioned pretension structural design can also be improved with considering electromagnetic performance. A statement should be addressed that the drawback of this method is that the procedure cannot handle both two circular polarizations simultaneously, which is also the drawback of other previous compensation methods.

4 Conclusions

- (1) Less iteration time and a little worse electromagnetic performance with maximum directivity in accuracy of 0.0001 dB than the exact one are provided by BFGS approximation Hessian matrix in the two-step structural design. A helpful guideline for the cable mesh reflector antennas design can be presented.
- (2) A tilt-like surface deformation to achieve a uniform phase distribution in reflector aperture for circularly polarized offset cable mesh reflector antennas is provided in the optimal structural design, and the electromagnetic performance including boresight directivity, beam squint angle, sidelobe levels and cross-polarization approaches better as the phase distribution becomes uniform.
- (3) Even though the other antenna electromagnetic performance besides boresight directivity is not added in the multidisciplinary optimization model, once the boresight directivity is optimized as its extremely maximum value with sufficiently small convergence criterion, the other performance will also be made as an acceptable value due to the electromagnetism property.

Open Access This article is distributed under the terms of the Creative Commons Attribution 4.0 International License (<http://creativecommons.org/licenses/by/4.0/>), which permits unrestricted use, distribution, and reproduction in any medium, provided you give appropriate credit to the original author(s) and the source, provide a link to the Creative Commons license, and indicate if changes were made.

References

1. HOFERER R A, RAHMAT-SAMII Y. Subreflector shaping for antenna distortion compensation: an efficient Fourier-Jacobi expansion with GO/PO analysis[J]. *IEEE Transactions on Antennas and Propagation*, 2002, 50(12): 1676–1687.
2. XU S, RAHMAT-SAMII Y. A novel beam squint compensation technique for circularly polarized conic-section reflector antennas [J] *IEEE Transactions on Antennas and Propagation*, 2010, 58(2): 307–317.
3. ENTEKHABI D, NJOKU E G, O'NEILL, et al. The soil moisture active passive (SMAP) mission[J]. *Proceedings of the IEEE*, 2010, 98(5): 704–716.
4. RAHMAT-SAMII Y, LEE S W. Vector diffraction analysis of reflector antennas with mesh surfaces[J]. *IEEE Transactions on Antennas and Propagation*, 1985, 33(1): 76–90.
5. MIURA A, RAHMAT-SAMII Y. Spaceborne mesh reflector antennas using complex weaves: extended PO/periodic-MoM analysis[J]. *IEEE Transactions on Antennas and Propagation*, 2007, 55(4): 1022–1029.
6. XU S, RAHMAT-SAMII Y, IMBRIALE W A. Subreflectarrays for reflector surface distortion compensation[J]. *IEEE Transactions on Antennas and Propagation*, 2009, 57(2): 364–372.
7. ADATIA N A, RUDGE A W. Beam squint in circularly polarized offset reflector antennas[J]. *Electronic Letter*, 1975, 11(21): 513–515.
8. DUAN D W, RAHMAT-SAMII Y. Beam squint determination in conic-section reflector antennas with circularly polarized feeds [J]. *IEEE Transactions on Antennas and Propagation*, 1991, 39 (5): 612–619.
9. EIHARDT K, WOHLLEBEN R, FIEBIG D. Compensation of the beam squint in axially symmetric, large dual reflector antennas with large-ranging laterally displaced feeds[J]. *IEEE Transactions on Antennas and Propagation*, 1990, 38(8): 1141–1149.
10. TANAKA H, SHIMOZONO N, and NATORI M C. A design method for cable network structures considering the flexibility of supporting structures[J]. *Trans. Japan Soc. Aero. Space Sci.*, 2008, 50(170): 267–273.
11. YANG B, SHI H, THOMSON M, et al. Optimal design of initial surface profile of deployable mesh reflectors via static modeling and Quadratic programming[C]/50th AIAA/ASME/ASCE/AHS/ASC/ Structures, Structural Dynamics, and Materials conference, Palm Springs, California, AIAA 2009-2173, May 4–7 2009: 1–9.
12. LIW W, LI D, YU X, JIANG J. Exact mesh shape design of large cable-network antenna reflectors with flexible ring truss supports [J]. *Acta Mechanica Sinica*, 2014, 30(2): 198–205.
13. MORTEROLLE S, MAURIN B, QUIRANT J, et al. Numerical form-finding of geotensoid tension truss for mesh reflector[J]. *Acta Astronautica*, 2012, 76: 154–163.
14. WANG Z, LI T, DENG H. Form-finding analysis and active shape adjustment of cable net reflectors with PZT actuators[J]. *Journal of Aerospace Engineering*, 2014, 27: 575–586.
15. DENG H, LI T, WANG Z. Pretension design for space deployable mesh reflectors under multi-uncertainty[J]. *Acta Astronautica*, 2015, 115, 270–276.
16. PADULA S L, ADELMAN H M, BAILEY M C, et al. Integrated structural electromagnetic shape control of large space antenna reflectors[J]. *AIAA Journal*, 1989, 27(6): 814–819.
17. ZHANG S, DU J, DUAN B, YANG G., et al. Integrated structural-electromagnetic shape control of cable mesh reflector antennas[J]. *AIAA Journal*, 2015, 53 (5): 1395–1398.
18. HEDGEPEETH J M. Accuracy potentials for large space antenna reflectors with passive structure[J]. *Journal of Spacecraft and Rockets*, 1982, 19(3): 211–217.
19. TIBERT A G, and PELLEGRINO S. Deployable tensegrity reflectors for small satellites[J]. *Journal of Spacecraft and Rockets*, 2002, 39(5): 701–709.
20. DATASHVILI L, BAIER H, SCHIMITSCHEK J, et al. High precision large deployable space reflector based on pillow-effect-free technology[C]/48th AIAA/ASME/ ASCE/AHS/ASC Structures, Structural Dynamics, and Materials Conference, Honolulu, Hawaii, 23–26 April 2007: 1–10.
21. TIBERT A G. Optimal design of tension truss antennas[C]/44th AIAA/ASME/ASCE/AHS/ASC Structures, Structural Dynamics, and Materials Conference and Exhibit, Norfolk, VA, 7–10 April, 2003: 1–11.
22. TRAN H C, LEE J. Form-finding of tensegrity structures with multiple states of self-stress[J]. *Acta Mech.*, 2011, 222, 131–147.
23. DU J, ZONG Y, BAO H. Shape adjustment of cable mesh antennas using sequential quadratic programming[J]. *Aerospace Science and Technology*, 2013, 30: 26–33.
24. ZHANG L., GUO F., LI Y. et al. Global dynamic modeling of electro-hydraulic 3-UPS/S parallel stabilized platform by bond graph [J]. *Chinese Journal of Mechanical Engineering*, 2016, 29(6): 1176–1185.
25. LIU S., DAO J., LI A., et al. Analysis of frequency characteristics and sensitivity of compliant mechanisms[J]. *Chinese Journal of Mechanical Engineering*, 2016, 29 (4): 680–693.

Shuxin ZHANG, born in 1987, is currently a lecturer at Key Laboratory of Electronic Equipment Structure Design of Ministry of Education, Xidian University, China. He received his PhD degree from Xidian University, China, in 2015. His research interests include integrated structural electromagnetic optimization design of cable mesh antennas and structural optimization. Tel: +86-29-88203040; E-mail: sxzhang@xidian.edu.cn

Jingli DU, is currently a professor at Key Laboratory of Electronic Equipment Structure Design of Ministry of Education, Xidian University, China. He received his PhD degree from Xidian University, China, in 2006. His research interests include mechanical analysis, optimization and control of flexible structures. Tel: +86-29-88203040; E-mail: jldu@mail.xidian.edu.cn

Wei WANG, born in 1980, is currently a professor at Key Laboratory of Electronic Equipment Structure Design of Ministry of Education, Xidian University, China. He received his PhD degree from Xidian University, China, in 2011. His main research interests include electromechanical coupling design of electric equipment, structural optimization design of large scale antennas and distortion prediction and compensation of antenna surface. Tel: +86-29-88203040; E-mail: wwang@xidian.edu.cn

Xinghua ZHANG, born in 1980, is currently a senior engineer at Qian Xuesen Laboratory of Space Technology, China Academy of Space Technology, China. He received his PhD degree from University of Science and Technology of China, in 2008. His main research interests include dynamic analysis of space structures and space solar power station design. Tel: +86-10-68113046; E-mail: zhangxinghua@qxslab.cn

Yali ZONG, born in 1988, is currently a lecturer at Key Laboratory of Electronic Equipment Structure Design of Ministry of Education, Xidian University, China. She received her PhD degree from Xidian University, China, in 2015. Her recent research interests include electromechanical synthetic design of cable-network antennas and structural optimization. Tel: +86-29-88203040; E-mail: zongyali_130@163.com